PAPER • OPEN ACCESS

Tomography of the QGP by heavy quarks

View the article online for updates and enhancements.

Related content

- A Short Course on Relativistic Heavy Ion Collisions: Signals of quark–gluon plasma
A K Chaudhuri

- A Short Course on Relativistic Heavy Ion Collisions: Equation of state for QGP and hadronic resonance gas
A K Chaudhuri

- A Short Course on Relativistic Heavy Ion Collisions: Introduction to the deconfined state
A K Chaudhuri

Tomography of the QGP by heavy quarks

T Song[1,2], **H Berrehrah**[1], **E L Bratkovskaya**[1,2,3], **D Cabrera**[1],
W Cassing[4], **J M Torres-Rincon**[1], **L Tolos**[1,5]

[1] Frankfurt Institute for Advanced Studies, University of Frankfurt, Frankfurt, Germany

[2] Institute for Theoretical Physics, University of Frankfurt, Frankfurt, Germany

[3] GSI Helmholtzzentrum für Schwerionenforschung GmbH, Darmstadt, Germany

[4] Institute for Theoretical Physics, University of Giessen, Giessen, Germany

[5] Institut de Ciencies de l'Espai (IEEC/CSIC), Universitat Autonoma de Barcelona, Spain

E-mail: E.Bratkovskaya@gsi.de

Abstract. The dynamics of partons and hadrons in ultra-relativistic nucleus-nucleus collisions is analyzed within the Parton-Hadron-String Dynamics (PHSD) transport approach, which is based on a dynamical quasiparticle model for the partonic phase (DQPM) including a dynamical hadronization scheme while reproducing lattice QCD results in thermodynamic equilibrium for the equation-of-state as well as transport coefficients like shear and bulk viscosities, the electric conductivity or the charm diffusion coefficient of the hot QCD medium. In this contribution we report on the recent results on the charm dynamics and elliptic flow in Au+Au collisions at RHIC and Pb+Pb reactions at the LHC as well as on the single electron spectra from $D-$ and $B-$meson semileptonic decays in Au+Au collisions at $\sqrt{s_{\rm NN}} =$200 and 62.4 GeV. We find that the PHSD approach well describes the $R_{\rm AA}$ and elliptic flow v_2 of open charm mesons in Au+Au collisions at $\sqrt{s_{\rm NN}} = 200$ GeV (from STAR) and 2.76 TeV (from ALICE) as well as the elliptic flow of single electrons at $\sqrt{s_{\rm NN}} = 200$ and 62.4 GeV (from PHENIX), however, the large $R_{\rm AA}$ at $\sqrt{s_{\rm NN}} = 62.4$ GeV is not reproduced at all which might indicate a new 'PHENIX puzzle'.

1. Introduction

The dynamics of the early universe in terms of the 'Big Bang' may be studied experimentally by ultra-relativistic nucleus-nucleus collisions at Relativistic-Heavy-Ion-Collider (RHIC) or Large-Hadron-Collider (LHC) energies in terms of 'tiny bangs' in the laboratory. With sufficiently strong parton interactions, the medium in the collision zone can be expected to achieve local equilibrium after some initial delay and exhibit approximately hydrodynamic flow [1, 2, 3]. In these collisions a new state of strongly interacting matter is created, being characterized by a very low shear viscosity η to entropy density s ratio, η/s, close to a nearly perfect fluid [4, 5]. Lattice QCD (lQCD) calculations [6, 7] indicate that a crossover region between hadron and quark-gluon matter should have been reached in these experiments.

Since the hot and dense matter produced in relativistic heavy-ion collisions appears only for a couple of fm/c, it is a big challenge for experiment to investigate its properties. The heavy flavor mesons are considered to be promising probes in this respect since the production of heavy flavor requires a large energy-momentum transfer. Thus it takes place early in the heavy-ion collisions, and - due to the large energy-momentum transfer - should be described by perturbative quantum chromodynamics (pQCD). The produced heavy flavor then interacts with the hot dense matter

(of partonic or hadronic nature) by exchanging energy and momentum. As a result, the ratio of the measured number of heavy flavors in heavy-ion collisions to the expected number in the absence of nuclear or partonic matter, which is the definition of R_{AA}, is suppressed at high transverse momentum, and the elliptic flow of heavy flavor is generated by the interactions in noncentral heavy-ion collisions. Although it had been expected that the R_{AA} of heavy flavor is less suppressed and its elliptic flow is smaller as compared to the corresponding quantities for light hadrons, the experimental data show that the suppression of heavy-flavor hadrons at high transverse momentum and its elliptic flow v_2 are comparable to those of light hadrons [8, 9]. This is a puzzle for heavy-flavor production and dynamics in relativistic heavy-ion collisions as pointed out by many groups [10, 11, 12]. For recent reviews we refer the reader to Refs. [13, 14].

Since the heavy-flavor interactions are closely related to the dynamics of the partonic or hadronic degrees-of-freedom due to their mutual interactions, a proper description of the relativistic heavy-ion collisions and their bulk dynamics is necessary. In this study we employ the parton-hadron-string dynamics (PHSD) approach, which differs from the conventional Boltzmann-type models [15, 16] in the aspect that the degrees-of-freedom for the QGP phase are off-shell massive strongly-interacting quasi-particles that generate their own mean-field potential [17]. The masses of the dynamical quarks and gluons in the QGP are distributed according to spectral functions whose pole positions and widths, respectively, are defined by the real and imaginary parts of their self-energies [18]. The partonic propagators and self-energies, furthermore, are defined in the dynamical quasiparticle model (DQPM) in which the strong coupling and the self-energies are fitted to lattice QCD results [19]. We recall that the PHSD approach has been successfully applied to p+A and Au+Au (Pb+Pb) collisions from SPS to LHC energies with respect to single-particle spectra, collective flows and electromagnetic observables [20, 21, 22].

2. Charm and bottom dynamics in PHSD
2.1. Initial heavy flavor production and fragmentation
In the PHSD the charm and bottom quark pairs are produced through initial hard nucleon-nucleon scattering in relativistic heavy-ion collisions. We employ the PYTHIA event generator [23] to produce the heavy-quark pairs and modify slightly their transverse momentum and rapidity such that they are similar to those from the FONLL calculations [24]. We recall that in the case of heavy-ion collisions at the top RHIC energy of $\sqrt{s} = 200$ GeV the transverse momentum and the rapidity of the charm quark are reduced by 10 % and 16 % [25], respectively, while those of the bottom quark are unmodified. The corrections employed at other ivariant energies can be found in Refs. [26, 27]. Accordingly, our tuned PYTHIA generator gives very similar charm and bottom distributions as those from FONLL calculations [24, 28], which fixes the input from pQCD in our approach.

The produced charm and bottom quarks in hard nucleon-nucleon interactions are hadronized in p+p collisions by emitting soft gluons, which is denoted by 'fragmentation'. We use the fragmentation function of Peterson which reads as [29]

$$D_Q^H(z) \sim \frac{1}{z[1 - 1/z - \epsilon_Q/(1-z)]^2},\tag{1}$$

where z is the momentum fraction of the hadron H fragmented from the heavy quark Q while ϵ_Q is a fitting parameter which is taken to be $\epsilon_Q = 0.01$ for charm [25] and 0.004 for bottom [30]. Since the charm quark is much heavier than the soft emitted gluons, it takes a large momentum fraction in the fragmentation into a $D-$meson. This is even more pronounced in the case of a bottom quark.

The excited $D^*(B^*)$ mesons first decay into $D(B) + \pi$ or $D(B) + \gamma$, and finally the $D-$ and $B-$mesons produce single electrons through the semileptonic decay [31]. This completes the

production and decay of heavy-flavor mesons in p+p collisions.

2.2. Shadowing in heavy-ion reactions

The production cross section for heavy-quark pairs in a nucleon-nucleon collision is calculated by convoluting the partonic cross section with the parton distribution functions (PDFs) of the nucleon [32]. However, the parton distribution functions are modified in a hadronic medium, i.e. suppressed at small momentum fraction x, slightly enhanced for $x \approx 0.1$ and then suppressed again for larger x (EMC effect). This is denoted as 'shadowing (antishadowing)' effect and is incorporated in the PHSD by employing the EPS09 package from Ref. [32] as in most of the related approaches [14]. The details of the implementation are given in Ref. [26].

2.3. Heavy-quark interactions in the QGP

In PHSD the baryon-baryon and baryon-meson collisions at high-energy produce strings. If the local energy density is above the critical energy density (~ 0.5 GeV/fm^3), the strings melt into quarks and antiquarks with masses determined by the temperature-dependent spectral functions from the DQPM [19]. Massive gluons are formed through flavor-neutral quark and antiquark fusion in line with the DQPM. In contrast to normal elastic scattering, off-shell partons may change their mass after the elastic scattering according to the local temperature T in the cell (or local space-time volume) where the scattering happens. This automatically updates the parton masses as the hot and dense matter expands, i.e. the local temperature decreases with time. The same holds true for the reaction chain from gluon decay to quark+antiquark ($g \to q + \bar{q}$) and the inverse reaction ($q + \bar{q} \to g$) following detailed balance.

The heavy quarks and antiquarks produced in early hard collisions - as described above - interact with the dressed lighter off-shell partons in the partonic phase. The cross sections for the heavy-quark scattering with massive off-shell partons have been calculated by considering explicitly the mass spectra of the final state particles in Refs. [33, 34, 35]. The elastic scattering of heavy quarks in the QGP is treated consistently in the PHSD by including the non-perturbative effects of the strongly interacting quark-gluon plasma (sQGP) constituents, i.e. the temperature-dependent coupling $g(T/T_c)$ as well as the effective propagators with broad spectral functions (imaginary parts) from the DQPM [19]. We recall that the divergence encountered in the t-channel scattering is cured self-consistently, since the infrared regulator is given by the finite DQPM gluon mass and width. We note that heavy flavor interactions in the QGP – as described by the DQPM charm scattering cross sections – differ substantially form the pQCD scenario [36], however, the spacial diffusion constant for charm quarks $D_s(T)$ is consistent with the lQCD data [26, 35]. For further details we refer the reader to Refs. [33, 34, 35].

2.4. Heavy-quark coalescence

The heavy-quark hadronization in heavy-ion collisions is realized via 'dynamical coalescence' and fragmentation. Here 'dynamical coalescence' means that the probability to find a coalescence partner is defined by Monte Carlo in the vicinity of the critical energy density $0.4 \leq \epsilon \leq 0.75$ GeV/fm^3 as explained below. We note that such a dynamical realization of heavy-quark coalescence is in line with the dynamical hadronization of light quarks in the PHSD and differs from the 'spontaneous' coalescence used in the early work [25] when heavy-quarks have been forced to hadronize at a critical energy density $\epsilon_c \approx 0.5$ GeV/fm^3 via coalescence or fragmentation by Monte Carlo. Indeed, the dynamical realization gives some window in energy density to find the proper light partner and leads to an enhancement of the heavy-quark fraction that hadronizes via coalescence.

In PHSD all antiquarks neighboring in phase space are candidates for the coalescence partner of a heavy quark. From the distances in coordinate and momentum spaces between the heavy

quark and light antiquark (or vice versa), the coalescence probability is given by [27]

$$f(\rho, \mathbf{k}_\rho) = \frac{8g_H}{6^2} \exp\left[-\frac{\rho^2}{\delta^2} - \mathbf{k}_\rho^2 \delta^2\right],$$ (2)

where g_H is the degeneracy of the heavy meson, and

$$\rho = \frac{1}{\sqrt{2}}(\mathbf{r}_1 - \mathbf{r}_2), \quad \mathbf{k}_\rho = \sqrt{2}\,\frac{m_2\mathbf{k}_1 - m_1\mathbf{k}_2}{m_1 + m_2},$$ (3)

with m_i, $\mathbf{r}_i$ and $\mathbf{k}_i$ denoting the mass, position and momentum of the quark or antiquark i in the center-of-mass frame, respectively. The width parameter δ is related to the root-mean-square radius of the produced heavy meson through

$$\langle r^2 \rangle = \frac{3}{2}\frac{m_1^2 + m_2^2}{(m_1 + m_2)^2}\delta^2.$$ (4)

Since this prescription gives a larger coalescence probability at low transverse momentum, the radius is taken to be 0.9 fm for a charm quark as well as for a bottom quark [25]. We also include the coalescence of charm quarks into highly excited states, $D_0^*(2400)^0$, $D_1(2420)^0$, and $D_2^*(2460)^{0,\pm}$ and the coalescence of bottom quarks into $B_1(5721)^{+,0}$, $B_2^*(5747)^{+,0}$, and $B(5970)^{+,0}$ which are, respectively, assumed to immediately decay to D (or D^*) and π and to B (or B^*) and π after hadronization as described in Ref. [25].

Summing up the coalescence probabilities from all candidates, whether the heavy quark or heavy antiquark hadronizes by coalescence or not, and which quark or antiquark among the candidates will be the coalescence partner, is decided by Monte Carlo. If a random number is above the sum of the coalescence probabilities, it is tried again in the next time step till the local energy density is lower than 0.4 GeV/fm^3, i.e. in the dominantly hadronic phase. The heavy quark or heavy antiquark, which does not succeed to hadronize by coalescence, then hadronizes through fragmentation as in p+p collisions.
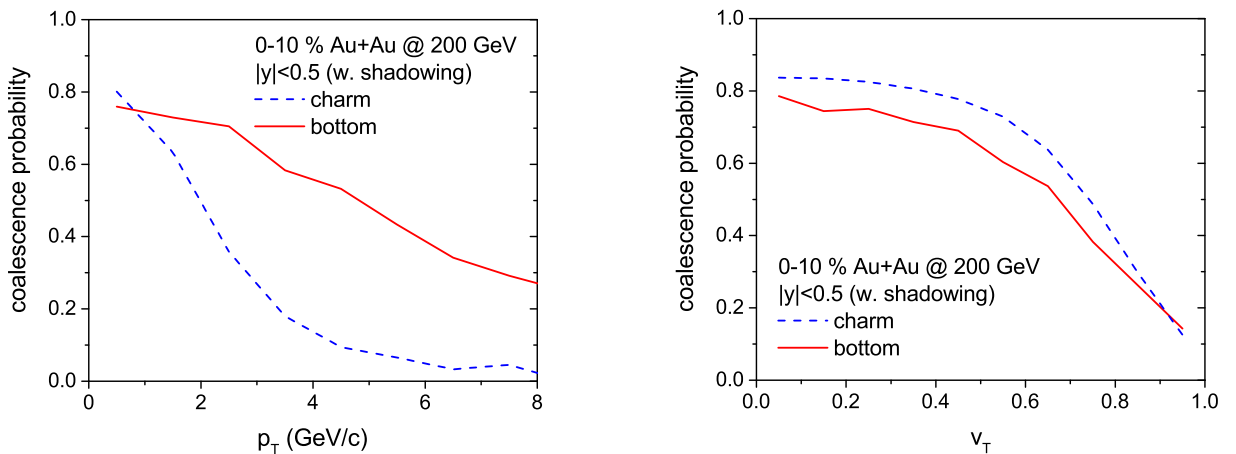

Figure 1. Coalescence probability of charm and bottom quarks at midrapidity ($|y| < 0.5$) as functions of transverse momentum (lhs) and of transverse velocity (rhs) in 0-10 % central Au+Au collisions at $\sqrt{s_{\mathrm{NN}}} = 200$ GeV taking into account the shadowing effect.

Fig. 1 shows the coalescence probabilities of charm and bottom quarks at midrapidity ($|y| < 0.5$) as functions of transverse momentum (lhs) and of transverse velocity (rhs) in 0-10 % central Au+Au collisions at $\sqrt{s_{\mathrm{NN}}} =$200 GeV. Since a heavy quark with a large transverse momentum has a smaller chance to find a coalescence partner close by in phase space, the coalescence probability decreases with increasing transverse momentum. It appears from the left panel of Fig. 1 that the coalescence probability of a bottom quark is larger than that of a charm quark. It emerges, however, because the bottom quark is much heavier than the charm quark. The right panel of Fig. 1 clearly shows that the coalescence probability is similar for a bottom or charm quark, when it is expressed as a function of the transverse velocity v_T (for $|y| < 0.5$).

2.5. Interactions of charm and bottom mesons with the hadronic medium
After the hadronization of heavy quarks and their subsequent decay into D, D^*, B and B^* mesons, the final stage of the evolution concerns the interaction of these states with the hadrons conforming the expanding bulk medium. A realistic description of the hadron-hadron scattering —potentially affected by resonant interactions— includes collisions with the states $\pi, K, \bar{K}, \eta, N, \bar{N}, \Delta, \bar{\Delta}$. Such a description of their interactions has been developed in Refs. [37, 38, 39] using effective field theory. Moreover, after the application of an effective theory, one has to implement to the tree-level scattering amplitudes a unitarization method to better control the behavior of the cross sections at moderates energies with potentially resonant scattering amplitudes.

The details of the interaction for the four heavy states follows quite in parallel by virtue of the "heavy-quark spin-flavor symmetry". It accounts for the fact that if the heavy masses are much larger than any other typical scale in the system, like Λ_{QCD}, temperature and the light hadron masses, then the physics of the heavy subsystem is decoupled from the light sector, and the former is not dependent on the mass nor on the spin of the heavy particle. This symmetry is exact in the ideal limit $m_Q \to \infty$, with m_Q being the mass of the heavy quark confined in the heavy hadron. In the opposite limit $m_Q \to 0$, one can exploit the chiral symmetry of the QCD Lagrangian to develop an effective realization for the light particles. This applies to the pseudoscalar meson octet $(\pi, K, \bar{K}, \eta)$. Although both symmetries are broken in nature (as in our approach, when implementing physical masses), the construction of the effective field theories incorporates the breaking of these symmetries in a controlled way. In particular, it provides a systematic expansion in powers of $1/m_H$ (inverse heavy-meson mass) and powers of p, m_l (typical momentum and mass of the light meson). For details the reader is referred to Refs. [37, 38, 39].

3. Results for heavy-ion reactions
So far we have described the interactions of the heavy flavor produced in relativistic heavy-ion collisions with partonic and hadronic degrees-of-freedom as well as their hadronization by coalescence or fragmentation. Since the matter produced in heavy-ion collisions is extremely dense, the interactions with the bulk matter suppresses heavy flavors at high-p_{T}. On the other hand, the partonic or nuclear matter is accelerated outward (exploding), and a strong flow is generated via the interactions of the bulk particles and the repulsive scalar interaction for the lighter partons. Since the heavy flavor strongly interacts with the expanding matter, it is also accelerated outwards. Such effects of the medium on the heavy-flavor dynamics are expressed in terms of the nuclear modification factor defined as

$$R_{\mathrm{AA}}(p_{\mathrm{T}}) \equiv \frac{dN_{\mathrm{AA}}/dp_{\mathrm{T}}}{N_{\mathrm{binary}}^{\mathrm{AA}} \times dN_{\mathrm{pp}}/dp_{\mathrm{T}}}, \tag{5}$$
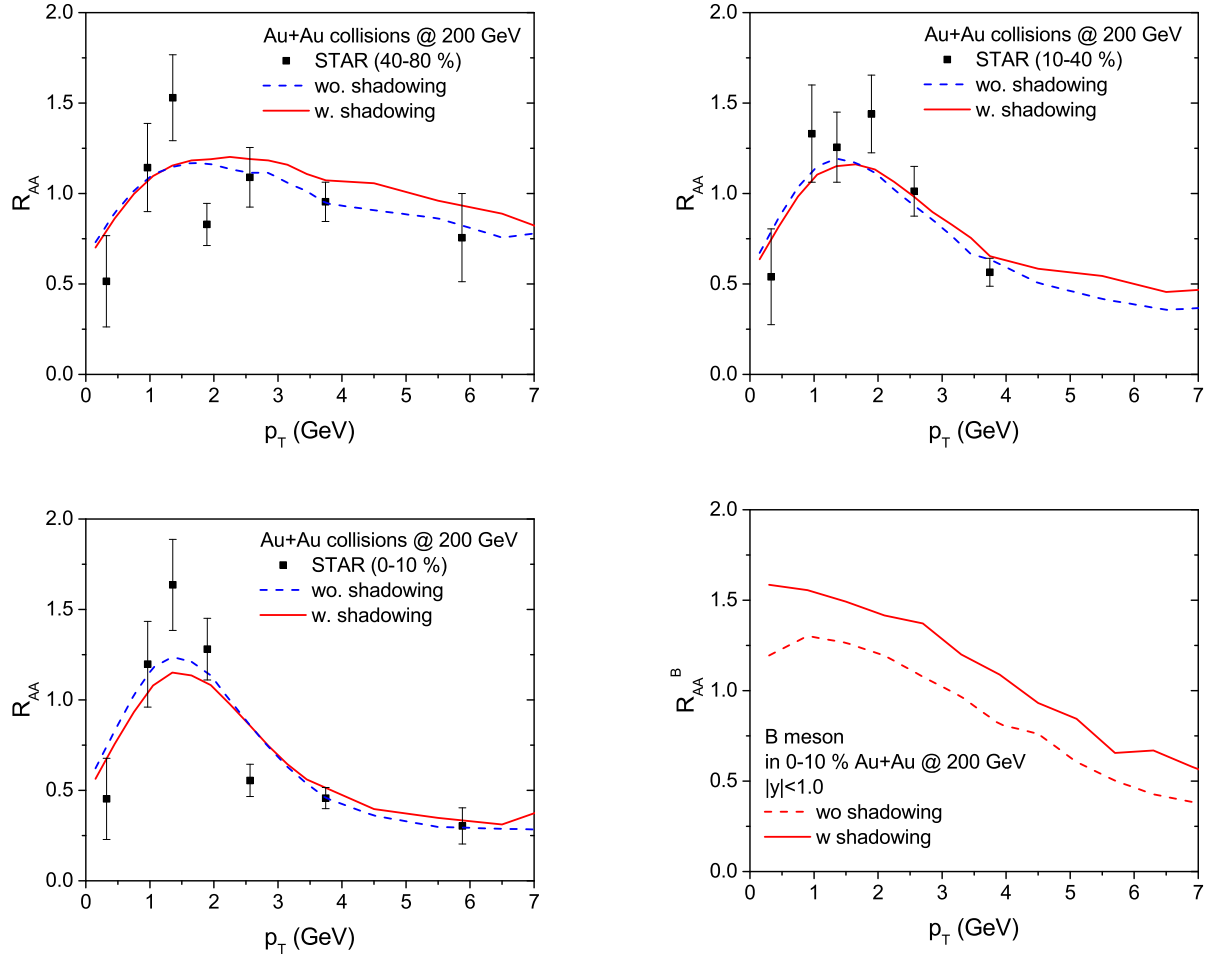
Figure 2. R_{AA} of $D-$mesons with (solid) and without (dashed) shadowing effect in Au+Au collisions at $\sqrt{s_{\mathrm{NN}}}$ =200 GeV for different centralities in comparison to the experimental data from the STAR collaboration [40]. (lower right panel) R_{AA} of $B-$mesons with (solid) and without (dashed) shadowing effect in central Au+Au collisions at $\sqrt{s_{\mathrm{NN}}}$ =200 GeV.

where N_{AA} and N_{pp} are, respectively, the number of particles produced in heavy-ion collisions and that in p+p collisions, and $N_{\mathrm{binary}}^{\mathrm{AA}}$ is the number of binary nucleon-nucleon collisions in the heavy-ion collision for the centrality class considered. Note that if the heavy flavor does not interact with the medium in heavy-ion collisions, the numerator of Eq. (5) will be similar to the denominator. For the same reason, an R_{AA} smaller (larger) than one in a specific p_{T} region implies that the nuclear matter suppresses (enhances) the production of heavy flavors in that transverse momentum region.

Furthermore, in noncentral heavy-ion collisions the produced matter expands anisotropically due to the different pressure gradients in plane and out-of plane. If the heavy flavor interacts strongly with the nuclear matter, then it also follows this anisotropic motion to some extend. The dominant anisotropic flow is expressed in terms of the elliptic flow v_2 which reads

$$v_2(\mathrm{p_T}) \equiv \frac{\int d\phi \cos 2\phi (dN_{\mathrm{AA}}/d\mathrm{p_T} d\phi)}{2\pi dN_{\mathrm{AA}}/d\mathrm{p_T}}, \tag{6}$$

where ϕ is the azimuthal angle of a particle in momentum space with respect to the reaction plane. In the following Subsections, we will present our results on the production of heavy flavors and single electrons in Au+Au (or Pb+Pb) collisions at different invariant energies.

3.1. Au+Au at $\sqrt{s_{\mathrm{NN}}}$ =200 GeV

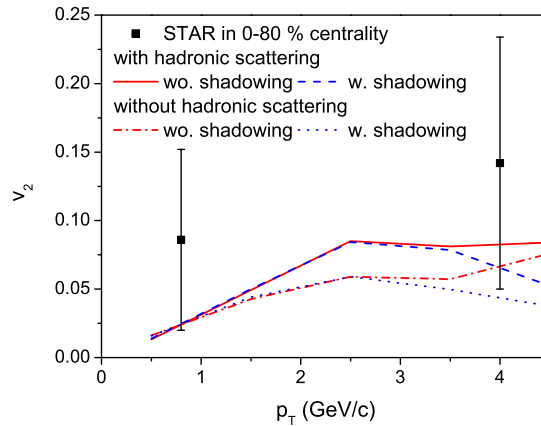We start with Au+Au collisions at the top RHIC energy and focus on the open charm mesons.

Figure 3. The elliptic flow v_2 of D^0 mesons with and without hadronic scattering and with and without shadowing in Au+Au collisions at $\sqrt{s_{\mathrm{NN}}}$ =200 GeV and 0-80% centrality. The experimental data are from the STAR Collaboration [40, 41].

In Fig. 2 we show the R_{AA} of $D-$mesons in different centrality classes with (solid) and without (dashed) shadowing effect in Au+Au collisions at $\sqrt{s_{\mathrm{NN}}}$ =200 GeV in comparison to the experimental data from the STAR collaboration [40]. Furthermore, we show in the lower right panel the R_{AA} of $B-$mesons in 0-10 % central Au+Au collisions at $\sqrt{s_{\mathrm{NN}}}$ =200 GeV from the PHSD calculations. The shadowing effect is excluded in the dashed lines and is included in the solid lines. We note that the R_{AA} of $D-$mesons without shadowing effect is slightly different from our previous results in Ref. [25], because the elastic backward scattering has been improved and the coalescence of charm quark takes place continuously in time as described above. As shown in Fig. 2, the shadowing effect decreases the charm production by $\sim$8 % in central reactions and increases the bottom production by $\sim$20 %. Apparently, the R_{AA} of $B-$mesons is much larger than that of $D-$mesons at the same transverse momentum. However, this is attributed to the larger bottom mass than charm mass as demonstrated in Fig. 1.

Fig. 3 displays the elliptic flow v_2 of D^0 mesons with and without hadronic scattering and with and without shadowing in 0-80% centrality Au+Au collisions at the top RHIC energy. We can see that the hadronic scattering plays an important role in the elliptic flow v_2 and enhances the v_2 of final D mesons by up to 30% at higher $\mathrm{p_T}$ essentially due to resonant scatterings [25]. The shadowing effect, furthermore, is ineffective up to $p_T \sim 3$ GeV/c.

3.2. Pb+Pb at $\sqrt{s_{\mathrm{NN}}}$ =2.76 TeV

Fig. 4 (lhs) shows the ratio R_{AA} of D^0, D^+, and D^{*+} mesons within the rapidity range $|y| < 0.5$ as a function of $\mathrm{p_T}$ in 0-10 % central Pb+Pb collisions at $\sqrt{s_{\mathrm{NN}}}$ =2.76 TeV. Here the charm quark mass is taken to be 1.5 GeV, independent of temperature. The solid and dotted lines are, respectively, the R_{AA} of D mesons with and without (anti-)shadowing. We can see that the R_{AA} of D mesons decreases especially at small transverse momentum due to shadowing. When
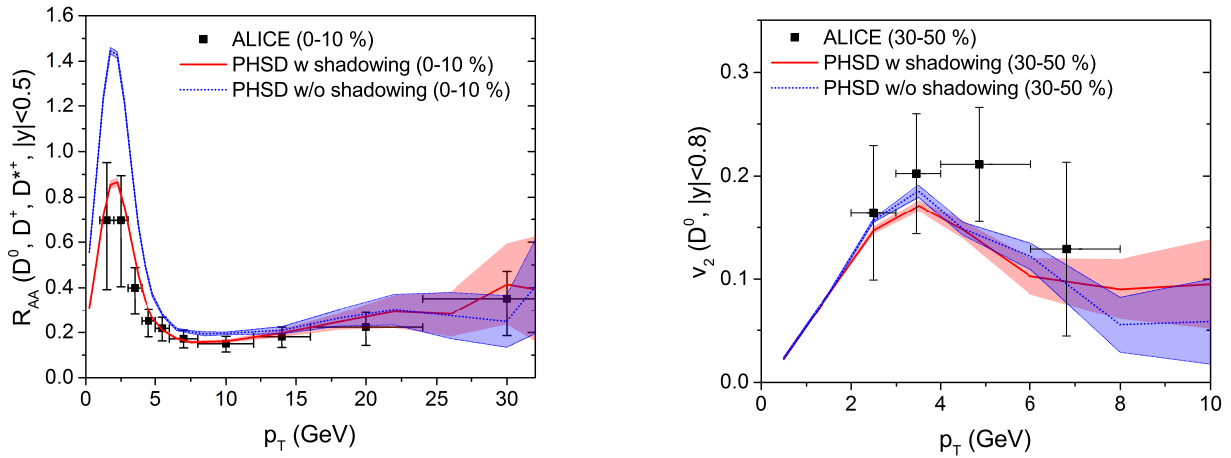
Figure 4. (lhs) The ratio R_{AA} of D^0, D^+, and D^{*+} mesons within $|y| < 0.5$ as a function of p_T in 0-10 % central Pb+Pb collisions at $\sqrt{s_{NN}}$ =2.76 TeV compared with the experimental data from the ALICE collaboration [42]. The solid and dotted lines are, respectively, R_{AA} with and without (anti-)shadowing. The charm quark mass is taken to be 1.5 GeV. (rhs) The elliptic flow v_2 of D^0 mesons within $|y| < 0.8$ in 30-50 % central Pb+Pb collisions at $\sqrt{s_{NN}}$ =2.76 TeV compared with the experimental data from the ALICE collaboration [44]. The solid (red) and dotted (blue) lines are, respectively, v_2 with and without (anti-)shadowing.

including shadowing our results are in a good agreement with the experimental data from the ALICE collaboration [42]. Since the radiative energy loss is not yet included in our study, it seems that the latter is not significant for transverse momenta up to 15 GeV/c (cf. Ref. [43]).

Fig. 4 (rhs) shows the elliptic flows v_2 of D^0 mesons within the rapidity range $|y| < 0.8$ in 30-50 % central Pb+Pb collisions at $\sqrt{s_{NN}}$ =2.76 TeV. The solid and dotted lines are, respectively, the results with and without (anti-)shadowing. Again the charm quark mass is taken to be 1.5 GeV. We can see that the PHSD results roughly reproduce the experimental data from the ALICE collaboration [44]. The (anti-)shadowing effect slightly decreases the elliptic flows, because it reduces the production of low-p_T charm which more easily follows the bulk flow. We recall that so far it has been a challenge for theoretical models to reproduce the experimental data and to explain simultaneously the large energy loss of charm quarks (R_{AA}) and the strong collectivity (v_2) [13]. According to the studies performed above the microscopic PHSD approach appears to be quite in line with the experimental observations for charm quarks at top RHIC and LHC energies.

3.3. Single electrons from Au+Au reactions at RHIC
The PHENIX Collaboration has measured the R_{AA} and elliptic flow of single electrons which emerge from charm and bottom decays. In this case it is important to include the bottom production and dynamics in the microscopic calculations since the single electrons from bottom decays become dominant at high p_T [13].

Fig. 5 shows the R_{AA} of single electrons from $D-$meson and $B-$meson semileptonic decays, which correspond to the dashed and dot-dashed lines, respectively, while the solid lines are the sum of them in 0-10 % central Au+Au collisions at $\sqrt{s_{NN}}$ =200 GeV. The PHSD calculations shown here include the shadowing effect, which enhances the bottom production and suppresses the charm production at low transverse momentum in line with the discussion above. We find that the single electrons from B decay have a larger contribution than that from D decay above
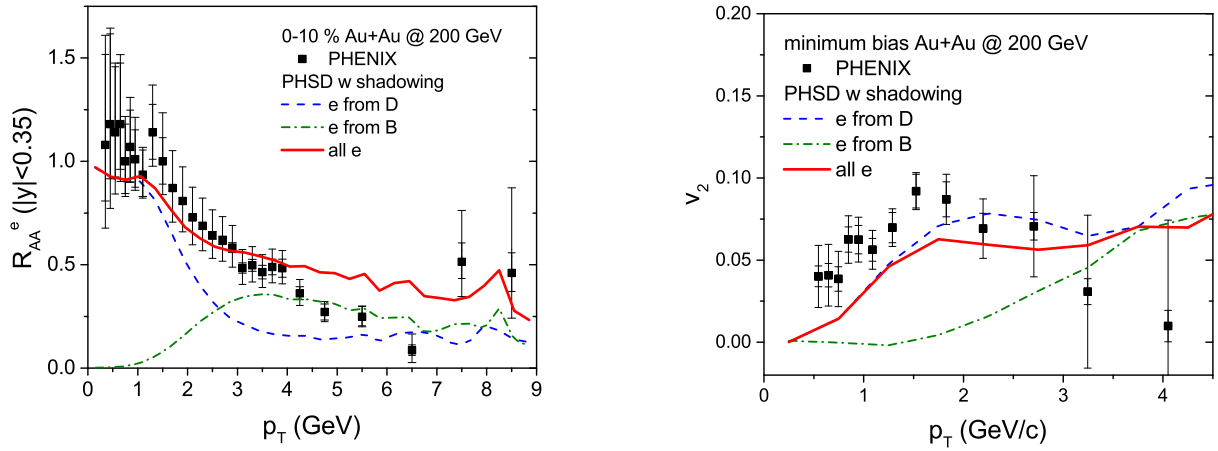
Figure 5. (lhs) R_{AA} of single electrons from the semi-leptonic decay of $D-$mesons (dashed) and of $B-$mesons (dot-dashed) and the sum of them (solid) with the shadowing effect included in 0-10 % central Au+Au collisions at $\sqrt{s_{NN}}$ =200 GeV in comparison to the experimental data from the PHENIX collaboration [48]. (rhs) The elliptic flow v_2 of single electrons from the semi-leptonic decay of $D-$mesons (dashed) and of $B-$mesons (dot-dashed) and of both of them (solid) with the shadowing effect included in minimum-bias Au+Au collisions at $\sqrt{s_{NN}}$ =200 GeV in comparison to the experimental data from the PHENIX collaboration [45].

$p_T \approx 2.7 - 2.8$ GeV. In p+p collisions, the contribution from B decay starts to be larger than that from D decay at about $p_T \approx 4$ GeV as shown in Ref. [25]. The reason for the dominance of B decay at lower transverse momentum in Au+Au collisions is that the R_{AA} of $B-$mesons is larger than that of $D-$mesons at high transverse momentum. In view of the results in Fig. 5 we may conclude that apart from the charm dynamics in Au+Au collisions at the top RHIC energy also the bottom dynamics is reasonably reproduced by the PHSD calculations.

The beam energy scan (BES) program at RHIC has been carried out by colliding Au nuclei at various energies down to $\sqrt{s_{NN}}$ =7.7 GeV. The aim of the program is to find information on the phase boundary and the critical point in the QCD phase diagram as pointed out in Refs. [46, 47]. It is expected that if the trajectories of the produced nuclear matter in the QCD phase diagram pass close to the critical point, some drastic changes of observables could be measured in experiments. Since the PHENIX collaboration recently measured the single electrons from heavy flavor decay at $\sqrt{s_{NN}}$ =62.4 GeV [48], which is much lower than the maximum energy at RHIC, we will also address this system in the present subsection.

Figs. 6 (lhs) and 6 (rhs) show, respectively, the R_{AA} and elliptic flow v_2 of single electrons from the semileptonic decay of heavy flavors in 0-20 % central Au+Au collisions at $\sqrt{s_{NN}}$ =62.4 GeV with the shadowing effect included. As at $\sqrt{s_{NN}}$ =200 GeV, the contribution from $D-$meson decay is important at low transverse momentum and superseeded by the contribution from B decay above 3 GeV in transverse momentum. The contribution from B decay becomes dominant at higher transverse momentum than at $\sqrt{s_{NN}}$ =200 GeV, because the ratio of the scattering cross section for bottom production to that for charm production is much lower at $\sqrt{s_{NN}}$ =62.4 GeV. The ratio is 0.75 % at $\sqrt{s_{NN}}$ =200 GeV and 0.145 % at $\sqrt{s_{NN}}$ =62.4 GeV according to the FONLL calculations [24].

The PHSD results in Fig. 6 (lhs) underestimate R_{AA} besides touching the lower error bars of the experimental data at low and high p_T. Although the shadowing effect enhances R_{AA} at low p_T, there is still a large discrepancy between the experimental data and our results in the range
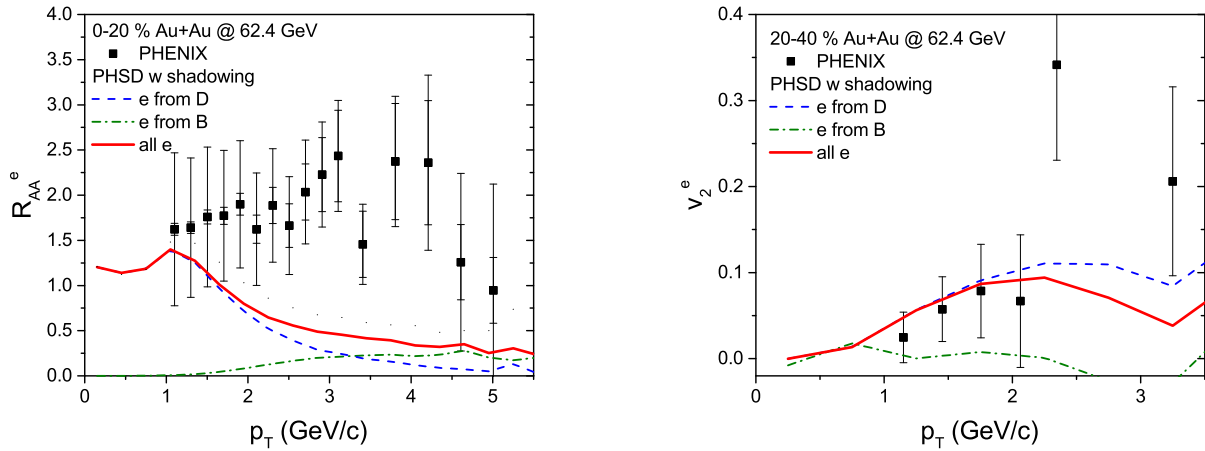
Figure 6. (lhs) R_{AA} of single electrons from the semi-leptonic decay of $D-$mesons (dashed) and of $B-$mesons (dot-dashed) and the sum of them (solid) with the shadowing effect included in 0-20 % central Au+Au collisions at $\sqrt{s_{\mathrm{NN}}}$ =62.4 GeV in comparison to the experimental data from the PHENIX collaboration [48]. (rhs) The elliptic flow v_2 of single electrons from the semi-leptonic decay of $D-$mesons (dashed) and of $B-$mesons (dot-dashed) and of both of them (solid) with the shadowing effect in 20-40 % central Au+Au collisions at $\sqrt{s_{\mathrm{NN}}}$ =62.4 GeV in comparison to the experimental data from the PHENIX collaboration [48].

of p_T between 2.5 and 4 GeV, which clearly lacks an explanation. We mention that a similar pattern of results has been shown in Ref. [49] and partially been attributed to the Cronin effect. We recall that the Cronin effect for the charm quarks is included in the PHSD via the EPS09 package used for the shadowing effect.

In spite of the difficulty in reproducing R_{AA}, the elliptic flow v_2 of single electrons at $\sqrt{s_{\mathrm{NN}}}$ =62.4 GeV is well described by the PHSD approach up to $p_T \approx 2$ GeV/c irrespective whether the shadowing effect is included or not, as shown in Fig. 6 (rhs). The v_2 of single electrons from $B-$meson decay is small at low transverse momentum for the same reason as at $\sqrt{s_{\mathrm{NN}}}$ =200 GeV.

4. Summary

In this contribution we have studied the dynamics of charm and bottom mesons as well as electron production through the semileptonic decay of heavy mesons in relativistic heavy-ion collisions at $\sqrt{s_{\mathrm{NN}}}$ =62.4, 200, and 2760 GeV within the PHSD transport approach. The ratio of the initial scattering cross section for bottom production to that for charm production at RHIC collision energies is less than 1 %. However, since the p_T spectrum of bottom quarks is harder than that of charm quarks and the single electrons from $B-$meson decay is much more energetic than that from $D-$meson decay, it is essential to take $B-$meson production into account in order to study the single electron production, especially at high p_T.

In analogy to the charm quark pairs, the bottom pairs are produced by using the PYTHIA event generator [23] which is tuned to reproduce the p_T spectrum and rapidity distribution of bottom quark pairs from the FONLL calculations [24]. The (anti)shadowing effect, which is the modification of the nucleon parton distributions in a nucleus, is implemented by means of the EPS09 package [32]. We have found that the (anti)shadowing effect is not so strong at RHIC energies as compared to LHC energies [26] where the shadowing becomes essential to find agreement with the experimental measurements especially at low p_T (cf. Fig. 4 (lhs)).

The charm and bottom partons - produced by the initial hard nucleon-nucleon scattering - interact with the massive quarks and gluons in the QGP by using the scattering cross sections calculated in the Dynamical Quasi-Particle Model (DQPM) which reproduces heavy-quark diffusion coefficients from lattice QCD calculations at temperatures above the deconfinement transition. When approaching the critical energy density for the phase transition from above, the charm and bottom (anti)quarks are hadronized into $D-$ and $B-$mesons through the coalescence with light (anti)quarks. Those heavy quarks, which fail in coalescence until the local energy density is below 0.4 GeV/fm^3, hadronize by fragmentation as in p+p collisions. The hadronized $D-$ and $B-$mesons then interact with light hadrons in the hadronic phase with cross sections that have been calculated in an effective lagrangian approach with heavy-quark spin symmetry. Finally, after freeze-out of the $D-$ and $B-$mesons they produce single electrons through semileptonic decays with the branching ratios given by the Particle Data Group (PDG) [31].

We have found that the coalescence probability for bottom quarks is still large at high p_T compared to charm quarks, and the R_{AA} of $B-$mesons is larger than that of $D-$mesons at the same (high) p_T. However, this can dominantly be attributed to the much larger mass of the bottom quark. If the coalescence probability and the R_{AA} are expressed as a function of the transverse velocity of the heavy quark, both charm and bottom coalescence become similar since both are comoving with the neighbouring light antiquarks (cf. Fig. 1).

Our studies show that the energy loss of D mesons at high p_T can be dominantly attributed to partonic scattering and that the collisional energy loss is dominant at least up to $p_T = 6$ GeV/c at top RHIC energies. The shape of R_{AA} versus p_T reflects the influence of quark coalescence and hadronic rescattering at low p_T while the D-meson elliptic flow v_2 gets enhanced sizeably by hadronic scattering [25]. Furthermore, both the R_{AA} and the elliptic flow of D mesons from the ALICE collaboration are reasonably reproduced (cf. Fig.4). This supports the validity and consistency of the PHSD approach for charm production and propagation in relativistic heavy-ion collisions in close analogy to our previous studies on electromagnetic probes from relativistic heavy-ion collisions [18].

Furthermore, we have found that the shadowing effect suppresses charm production preferentially at small transverse momentum and mid-rapidity, and it helps the PHSD to reproduce the ratio R_{AA} of D mesons from the ALICE collaboration at LHC energies. The shadowing also slightly decreases the elliptic flow of D mesons because it suppresses the production of charm quarks with small transverse momentum which more easily follow the bulk flow.

Finally, we found that the PHSD approach can roughly reproduce the experimental data on single electron production in Au+Au collisions at $\sqrt{s_{NN}}=200$ – including essential contributions from bottom decay – and the elliptic flow of single electrons at $\sqrt{s_{NN}}=62.4$ GeV from the PHENIX collaboration. However, the R_{AA} at $\sqrt{s_{NN}}=62.4$ GeV is clearly underestimated which presently remains as an open puzzle.

5. References

[1] Ollitrault J Y 1992 *Phys. Rev.* D **46** 229
[2] Heinz U and Kolb P 2002 *Nucl. Phys.* A **702** 269
[3] Shuryak E V 2009 *Prog. Part. Nucl. Phys.* **62** 48
[4] Shuryak E V 2005 *Nucl. Phys.* A **750** 64
[5] Gyulassy M and McLerran L 2005 *Nucl. Phys.* A **750** 30
[6] Cheng M *et al.* 2008 *Phys. Rev.* D **77** 014511
[7] Aoki Y *et al.* 2009 *JHEP* **0906** 088
[8] Abelev B *et al.* [ALICE Collaboration] 2012 *JHEP* **1209** 112
[9] Abelev B *et al.* [ALICE Collaboration] 2013 *Phys. Rev. Lett.* **111** 102301
[10] Das S K Scardina F Plumari S Greco V 2015 *Phys. Lett.* B **747** 260
[11] Nahrgang M Aichelin J Gossiaux P B Werner K 2016 *Phys. Rev.* C **93** 044909
[12] Aichelin J Gossiaux P B Gousset T 2014 *Phys. Rev.* D **89** 074018
[13] Andronic A *et al.* 2016 *Eur. Phys. J.* C **76** 107
[14] Primo F Rapp R 2016 *arXiv*:1603.00529
[15] Plumari S Puglisi A Scardina F and Greco V 2012 *Phys. Rev.* C **86** 054902
[16] Xu Z and Greiner C 2005 *Phys. Rev.* C **71** 064901
[17] Cassing W and Bratkovskaya E L 2009 *Nucl. Phys.* A **831** 215
        Bratkovskaya E L *et al.* 2011 *Nucl. Phys.* A **856** 162
[18] Linnyk O Bratkovskaya E Cassing W 2016 *Prog. Part. Nucl. Phys.* **87** 50
[19] Cassing W 2009 *Eur. Phys. J. ST* **168** 3
        Cassing W 2007 *Nucl. Phys.* A **795** 70
[20] Linnyk O Cassing W and Bratkovskaya E L 2014 *Phys.Rev.* C **89** 034908
        Linnyk O Konchakovski V P Cassing W and Bratkovskaya E L 2013 *Phys. Rev.* C **88** 034904
        Linnyk O Konchakovski V Steinert T Cassing W Bratkovskaya E L 2015 *Phys. Rev.* C **92** 054914
[21] Konchakovski V P *et al.* 2012 *Phys. Rev.* C **85** 044922
[22] Konchakovski V P Cassing W and Toneev V D 2015 *J. Phys. G* **42** 055106
[23] Sjostrand T Mrenna S Skands P Z 2006 *JHEP* **0605** 026
[24] Cacciari M Frixione S Houdeau N Mangano M L Nason P Ridolfi G 2012 *JHEP* **1210** 137
[25] Song T Berrehrah H Cabrera D Torres-Rincon J M Tolos L Cassing W Bratkovskaya E 2015 *Phys. Rev.* C **92** 014910
[26] Song T Berrehrah H Cabrera D Cassing W Bratkovskaya E 2016 *Phys. Rev.* C **93** 034906
[27] Song T Berrehrah H Cabrera D Torres-Rincon J M Tolos L Cassing W Bratkovskaya E 2016 *arXiv*:1605.07887
[28] Cacciari M Nason P Vogt R 2005 Phys. Rev. Lett. **95** 122001
[29] Peterson C Schlatter D Schmitt I Zerwas P M 1983 *Phys. Rev.* D **27** 105
[30] Abdallah J *et al.* [DELPHI Collaboration] 2011 *Eur. Phys. J.* C **71** 1557
[31] Olive K A *et al.* [Particle Data Group Collaboration] 2014 *Chin. Phys. C* **38** 090001
[32] Eskola K J Paukkunen H Salgado C A 2009 *JHEP* **0904** 065
[33] Berrehrah H Bratkovskaya E Cassing W Gossiaux P B Aichelin J Bleicher M 2014 *Phys. Rev.* C **89** 054901
[34] Berrehrah H Gossiaux P B Aichelin J Cassing W Bratkovskaya E 2014 *Phys. Rev.* C **90** 064906
[35] Berrehrah H Bratkovskaya E Steinert T Cassing W 2016 *Int. Journal of Mod. Phys.* E **25** 1642003
[36] Berrehrah H *et al.* 2016 *arXiv*:1604.02343 [hep-ph]
[37] Tolos L Torres-Rincon J M 2013 *Phys. Rev.* D **88** 074019
[38] Torres-Rincon J M Tolos L Romanets O 2014 Phys. Rev. D **89** 074042
[39] Tolos L 2013 *Int. J. Mod. Phys.* E **22** 1330027
[40] Adamczyk L *et al.* [STAR Collaboration] 2014 *Phys. Rev. Lett.* **113** 142301
[41] Tlusty D [STAR Collaboration] 2013 *Nucl. Phys.* A **904-905** 639c
[42] Adam J *et al.* [ALICE Collaboration] 2015 *arXiv*:1509.06888 [nucl-ex]
[43] Cao S Qin G Y Bass S A 2015 *Phys. Rev.* C **92** 054909
[44] Abelev B B *et al.* [ALICE Collaboration] 2014 *Phys. Rev.* C **90** 034904
[45] Adare A *et al.* [PHENIX Collaboration] 2007 *Phys. Rev. Lett.* **98** 172301
[46] Mohanty B [STAR Collaboration] 2011 *J. Phys. G* **38** 124023
[47] Kumar L [STAR Collaboration] 2011 *J. Phys. G* **38** 124145
[48] Adare A *et al.* [PHENIX Collaboration] 2015 *Phys. Rev.* C **91** 044907
[49] He M Fries R J Rapp R 2015 *Phys. Rev.* C **91** 024904